Realization of High-Fidelity Perfect Entanglers between Remote Superconducting Quantum Processors

Juan Song,[1,2,3,*] Shuang Yang,[1,*] Pei Liu,[1,4,*] Hui-Li Zhang,[1] Guang-Ming Xue,[1,5] Zhen-Yu Mi,[1,†] Wen-Gang Zhang,[1,‡] Fei Yan,[1] Yi-Rong Jin,[1,§] and Hai-Feng Yu[1,5]

[1]*Beijing Key Laboratory of Fault-Tolerant Quantum Computing, Beijing Academy of Quantum Information Sciences, Beijing 100193, China*

[2]*Beijing National Laboratory for Condensed Matter Physics and Institute of Physics, Chinese Academy of Sciences, Beijing 100190, China*

[3]*University of Chinese Academy of Sciences, Beijing 101408, China*

[4]*State Key Laboratory of Low Dimensional Quantum Physics and Department of Physics, Tsinghua University, Beijing 100084, China*

[5]*Hefei National Laboratory, Hefei 230088, China*

(Received 8 October 2024; revised 2 April 2025; accepted 8 July 2025; published 30 July 2025)

Superconducting qubit systems, one of the leading candidates for universal quantum computing, face scalability challenges such as frequency crowding, wiring complexity, and packaging problems. Distributed quantum computing offers a viable strategy for constructing larger quantum information processing systems. Yet, direct universal quantum gates between remote qubits—critical to distributed architectures—remain unrealized. Here, we demonstrate direct high-fidelity entangling gates between two remote superconducting quantum processors separated by a 30 cm distance, utilizing standing-wave modes in their connecting coaxial cable. We achieve cross-entropy benchmarking fidelities of $(99.15 \pm 0.02)\%$ and $(98.03 \pm 0.04)\%$ for the controlled-NOT and controlled-Z gates, respectively, outperforming state transfer and feedback-based protocols in fidelity and efficiency. This advancement significantly enhances the prospect of universal distributed quantum information processing, which is the critical step toward future large-scale quantum systems.

DOI: 10.1103/npr7-b7kq

Introduction—Superconducting quantum processors have demonstrated their advantage in quantum computation and simulation over classical computers, particularly as the number of qubits surpasses the order of 100 [1–5]. Significantly larger quantum processors with ∼50 million qubits are necessary to execute practical algorithms with quantum error correction [6]. Fabricating such a large-scale quantum processor on a single chip is challenging due to various limitations, including unavoidable chip modes and package modes, frequency crowding, wiring problems, etc. [7]. Meanwhile, planar connectivity also increases the demand for the number of qubits and the depth of circuits when implementing quantum algorithms and quantum error correction [8]. Thus, distributed quantum computing has garnered significant interest, as it offers a viable solution for scaling up quantum processors by linking multiple small-scale processors to facilitate large-scale quantum computing [9–13]. The key to implementing universal quantum computation in distributed quantum systems lies in realizing the essential element of the universal gate set, the two-qubit gate, between different processors [14]. Recent studies on the quantum state transfer (QST) process have demonstrated that employing superconducting transmission lines to link small processors offers a feasible way to scale superconducting quantum computation [15–23]. However, the QST process mediated by flying photons or auxiliary cavities requires the target qubit to be kept in its ground state, which cannot deal with the superposition case and thus cannot directly form a two-qubit gate. Meanwhile, the unitarity and accuracy of the QST process suffer from the undesired excitations. The unitary perfect entangler [24,25], with the maximal entangling power [26], is necessary to form a universal gate set. The QST-based two-qubit gate remained elusive until researchers successfully demonstrated a protocol leveraging two ancillary qubits combined with quantum feedback control [27]. A recent theoretical investigation in Ref. [28] has explored realizing an entangling gate between two

*These authors contributed equally to this work.
†Contact author: mizy@baqis.ac.cn
‡Contact author: zhangwg@baqis.ac.cn
§Contact author: jinyr@baqis.ac.cn

Published by the American Physical Society under the terms of the Creative Commons Attribution 4.0 International license. Further distribution of this work must maintain attribution to the author(s) and the published article's title, journal citation, and DOI.

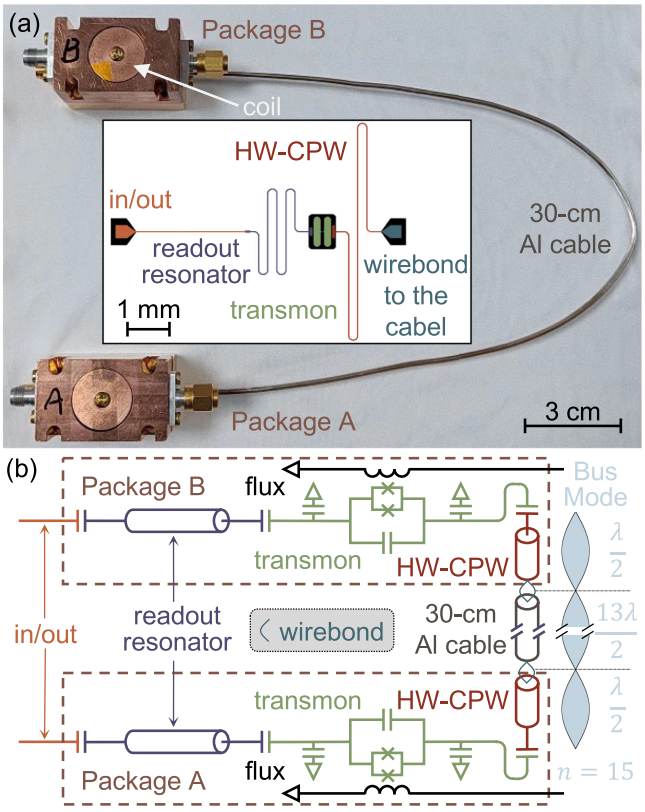


FIG. 1. Photograph of and circuit schematic for the remotely coupled system. (a) Photograph showing the two packages connected by a superconducting coaxial cable. Each copper sample holder has a small coil installed inside each package and beneath the chip. Inset: layout of one chip that consists of a transmission line (orange), a resonator (purple), a transmon (green), and a half-wavelength coplanar waveguide (HW-CPW, red). (b) The circuit schematic, and the 15th standing-wave mode of current inside the cable.

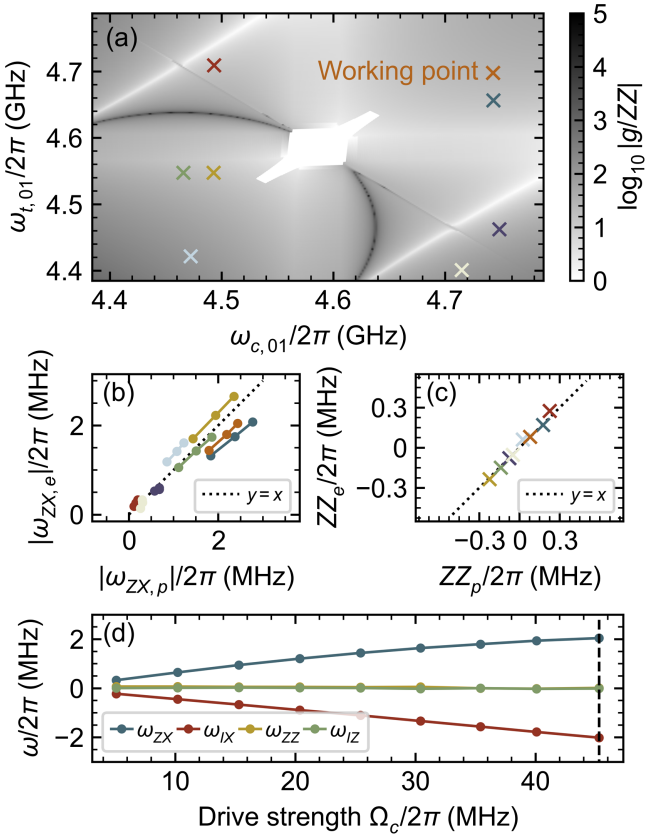


FIG. 2. Experimental and simulated results of the cross-resonance effect and residual ZZ interaction. (a) The ratio of the effective coupling strength g to the ZZ-interaction strength when coupled via single mode $n = 15$. The central white area is excluded from simulations because the frequencies of the qubits and bus mode $n = 15$ are nearly degenerate. (b) Considering modes $n = 14$, 15, 16 (when 16 is inferred), the CR interaction strength $|\omega_{ZX,p}|$ is predicted by simulations and compared with the experimental $|\omega_{ZX,e}|$ at different frequencies for the two qubits and three drive strengths. (c) The residual ZZ-interaction strengths. The different working frequencies are labeled by corresponding colors in (a), (b), and (c). (d) The CR interaction strength $|\omega_{ZX}|$ as a function of driving strength Ω_c at the working point. The dashed line indicates the selected drive strength.

remotely connected quantum processors via the cross-resonance (CR) effect [29–33]. Furthermore, the ac Stark-induced ZZ interaction [33,34] can also be employed to implement a remote entangling gate directly.

In this Letter, we report the realization of direct two-qubit entangling gates between two separately packaged quantum processors. Unlike the feedback-based protocol [27] that typically requires a longer time (> 1.8 μs) and may have lower fidelity (70.2%), our remote gates exhibit both short duration [204 ns for controlled-NOT (CNOT), and 430 ns for controlled-Z (CZ)] and high fidelity (99.15% for CNOT, and 98.03% for CZ). It does not require feedback control and extra qubits. We use cross-entropy benchmarking (XEB) to benchmark the two-qubit gates and implement a Bell-inequality test to confirm those unitary operations. The proposed approach also enables intrachip connections, presenting potential routes to implement error correction codes with higher coding density [8]. These advancements provide an efficient and universal protocol to implement distributed quantum information processing, paving the way for sophisticated large-scale quantum engineering in the future.

Experiment system and results—Our processor shown in Fig. 1(a) consists of two packages [Fig. 1(b) shows the circuit schematic]. Each package contains one transmon qubit, whose frequency can be tuned by the magnetic flux generated by the coil. The transmon qubit is capacitively coupled to a readout resonator and a half-wavelength coplanar waveguide (HW-CPW). The other end of the HW-CPW is wire-bonded to a 30-cm-long aluminum (Al) coaxial cable with Al wires. In our experiment, the 15th current standing-wave mode is mainly used for mediating the interaction. Thus, our design aligns the wave node with the bonding joint to reduce the wire-bond-induced channel loss [19]. The two packages are shielded with a cryogenic μ

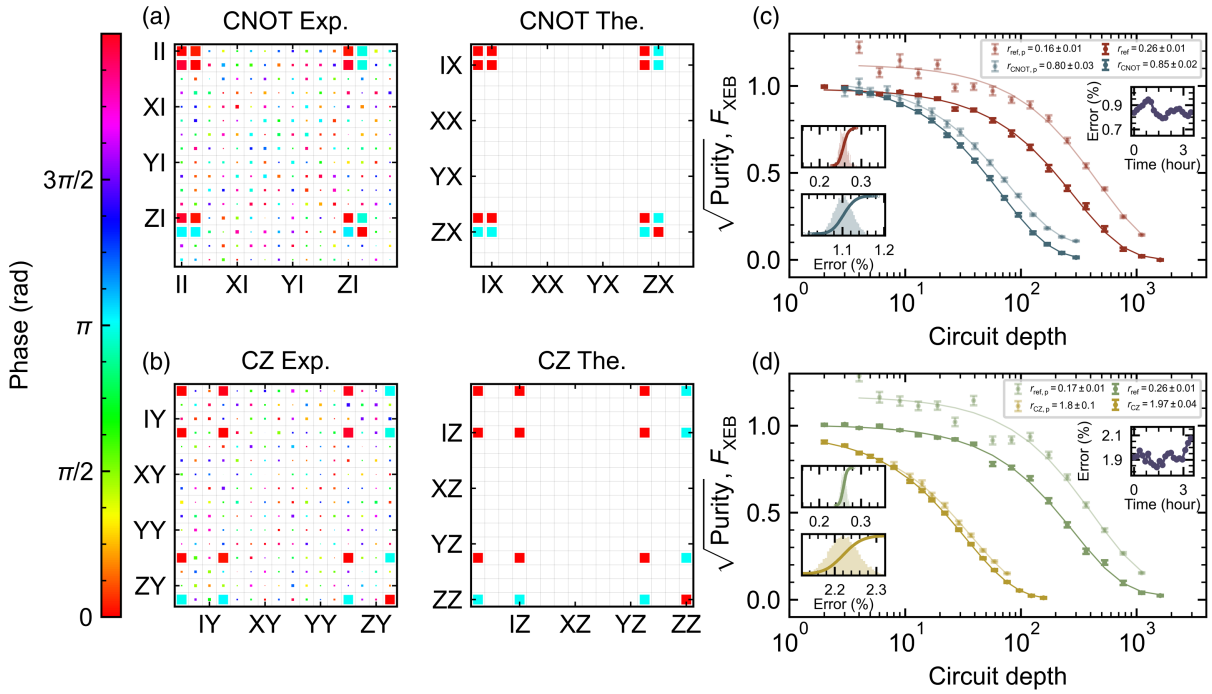


FIG. 3. Quantum process tomography (QPT) and cross-entropy benchmarking (XEB). The quantum process matrix of the experimental (a) CNOT [(b) CZ] gate, along with its theoretical matrix with QPT fidelity $F = 98.72\%$ ($F = 96.01\%$). The elements of each complex matrix are shown by colored squares, whose area indicates the ratio of the absolute value to 0.5 while color indicates the phase. The XEB fidelities (dark color) and purities (light color) of circuits are shown in (c) and (d), respectively. The left insets are histograms of the error rates of joint single-qubit gates and joint single-qubit gates with two-qubit gates calculated by bootstrapping. The two-qubit gate error rates are calculated from the two cases. The right insets display the time stability of gate error rates.

metal can to reduce the impact of magnetic flux fluctuations and then mounted onto the mixing chamber cold plate of a dilution refrigerator [see Supplemental Material (SM) [35]].

The system Hamiltonian is given by

$$H = \sum_{i=c,t}\left(\omega_i a_i^\dagger a_i + \frac{\alpha_i}{2} a_i^\dagger a_i^\dagger a_i a_i\right) + \sum_n \omega_n a_n^\dagger a_n + \sum_n g_{c,n}\left(a_c^\dagger + a_c\right)\left(a_n^\dagger + a_n\right) + \sum_n (-1)^n g_{t,n}\left(a_t^\dagger + a_t\right)\left(a_n^\dagger + a_n\right), \quad (1)$$

with the transmons described by Duffing oscillators. Here, $a^\dagger$ and a are the creation and annihilation operators, respectively. $g_{c,n}$ ($g_{t,n}$) is the coupling strength between the control (target) qubit and the standing-wave mode n (the nth bus mode). From the measured spectra of both qubits, we observe several equidistant anticrossing points, indicating the interaction between the qubits and the bus modes. By fitting the spectra in the anticrossing region, we extract ω_n and $g_{c(t),n}$ (see SM [35]). Assuming all the bus modes are in their ground state, the effective coupling strength g and the residual ZZ-interaction strength between two qubits are of primary concern. A simple simulation result with only one bus mode $n = 15$ is considered and shown in Fig. 2(a), with parameter details and additional simulation results provided in SM [35]. Guided by the numerical simulation results, we choose working frequencies of the control and target qubits that yield weak ZZ interaction, strong coupling strength, and weak spectator effect of the bus modes. Here, we emphasize that the flux bias is used solely for determining the working point. Therefore, we treat our qubits as fixed-frequency and do not apply any flux pulse throughout the experiment.

The CR-based gate is one of the most widely employed gates to generate entanglement in fixed-frequency qubit systems [4,28]. Phenomenologically, we express the effective two-qubit CR driving Hamiltonian in terms of IX, IY, IZ, ZX, ZY, and ZZ,

$$H_{\text{eff}} = \omega_{IX} IX + \omega_{IY} IY + \omega_{IZ} IZ + \omega_{ZX} ZX + \omega_{ZY} ZY + \omega_{ZZ} ZZ, \quad (2)$$

where X, Y, and Z are the Pauli matrices and I is the identical matrix. Based on the simulation results, we set the transition frequency of the control and target qubit to $\omega_c/2\pi = 4.743$ and $\omega_t/2\pi = 4.698$ GHz, respectively, to suppress the residual ZZ interaction. Using the Hamiltonian tomography method in Ref. [31], we extract the six CR interaction strengths in Eq. (2). Then, we vary the driving amplitude Ω_c (the equivalent Rabi frequency)

and obtain $|\omega_{ZX}|$ as a function of the driving amplitude, as shown in Fig. 2(d). Together with several different frequencies of the control and target qubits, $|\omega_{ZX,e}|$ and residual ZZ-interaction strength ZZ_e extracted from the experimental data (with subscript "e") are compared with the simulation predicted ones (with subscript "p"), as shown in Figs. 2(b) and 2(c). The simulation results considering three bus modes agree well with the experimental results, indicating that the coupling between two qubits in the dispersive regime is contributed by several related bus modes simultaneously (see SM [35]).

It is noticed that controlled-X $(\mathrm{CX}) = \exp[-i\pi(ZX - IX)/4]$ and $\mathrm{CNOT} = e^{-i\pi/4} \cdot \mathrm{CX} \cdot \exp(-i\pi ZI/4)$. Then, we fine-tune the driving parameters to cancel the unwanted IY, ZY, IZ interactions, and set $\omega_{IX} = -\omega_{ZX}$, leading to a CNOT gate with negligible ZZ interaction [31]. When the driving frequency is detuned properly, the X-like, Y-like interactions vanish under the rotating wave approximation, the ZZ interaction becomes dominant. To realize the CZ gate, we simultaneously apply a microwave drive to both qubits at a frequency of $\omega_d/2\pi = 4.667$ GHz. The operation relies on conditional phase accumulation, where the target qubit acquires a state-dependent phase shift determined by the control qubit. By maintaining a fixed driving amplitude and optimizing the pulse duration, we ensure that the phase difference reaches π. This results in the desired π-phase shift exclusively on the $|11\rangle$ state, thereby implementing the CZ gate with high fidelity. The calibration protocols are described in SM [35].

Quantum process tomography (QPT) and XEB are employed to benchmark the performance of the calibrated CNOT and CZ gates. The QPT χ matrices are extracted and compared to the ideal χ_{CNOT} and χ_{CZ}, as shown in Fig. 3(a) and 3(b). The process fidelity is estimated to be $F_{\mathrm{CNOT}} = \mathrm{Tr}(\chi \cdot \chi_{\mathrm{CNOT}}) = 98.72\%$ and $F_{\mathrm{CZ}} = 96.01\%$. The state preparation and measurement (SPAM) error influences the QPT fidelity. Therefore, the SPAM-independent XEB method is implemented [36]. By fitting the decay rate of the XEB fidelity as the number of CNOT (CZ) gates, shown in Figs. 3(c) and 3(d), the average error rate of our CNOT (CZ) gate is $(0.85 \pm 0.02)\%$ $((1.97 \pm 0.04)\%)$ with a gate duration of 204 ns (430 ns). Following the method in Ref. [1], we extract the purity information from the XEB results. The purity error is estimated to be $(0.80 \pm 0.03)\%$ $[(1.8 \pm 0.1)\%]$ per CNOT (CZ) gate, contributing 94% (91%) of the average error rate.

Finally, we demonstrate the establishment of remote entanglement between the two packages by testing the violation of the Bell inequality. We prepare the system in one of the Bell states $|\Phi^+\rangle = (|00\rangle + |11\rangle)/\sqrt{2}$, which is shown in Fig. 4(b) with a fidelity of 99.14% (81.79% without readout error correction, the decrease of the fidelity is due to the SPAM error that agrees with the analysis in SM [35]). We then perform the Clauser-Horne-Shimony-Holt form of the Bell-inequality test [42] on our remotely entangled state, with the Clauser-Horne-Shimony-Holt correlation S shown in Fig. 4(a). The control (target) qubit is measured in two orthogonal bases α and $\alpha_\perp$ (β and $\beta_\perp$), simultaneously. By scanning the angle θ between α and β, the maximum $S = 2.15 \pm 0.04$ exceeds the classical limit 2 by 3.8 standard deviations at $\theta = 5\pi/4$. After readout correction, the maximum correlation S is calculated to be 2.88 ± 0.05, which is slightly higher than the quantum limit $2\sqrt{2}$. The excess mainly comes from the initialization error on the two qubits (see SM [35]).

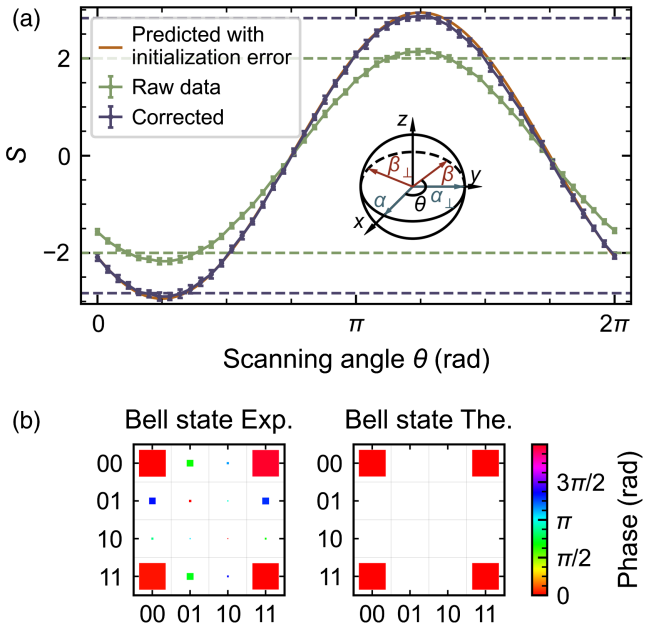


FIG. 4. Bell-inequality measurement and Bell state preparation. (a) The Clauser-Horne-Shimony-Holt correlation S as a function of the scanning angle θ. The green dots indicate the data without readout correction, and the purple ones represent the data under readout correction. Horizontal dashed lines denote classical and quantum limits. The red line indicates the experimentally measured data predicted with initialization error. (b) The experimental and theoretical density matrices of the Bell state $|\Phi^+\rangle$ with fidelity $F = 99.14\%$. The area of each square corresponds to the ratio of the absolute value of each complex element to 1.

Conclusion—We investigate the coupling mechanism of the remotely coupled system and fine-tune the driving parameters to realize CNOT and CZ gates between two separately packaged quantum processors. The average fidelity characterized by the XEB method is $(99.15 \pm 0.02)\%$ for the CNOT gate and $(98.03 \pm 0.04)\%$ for the CZ gate. With its high fidelity, our hardware-efficient approach requires no extra qubits, no postselection or feedback control, making it highly hardware-efficient, low-latency, and engineering-friendly. These advancements mark a significant step towards scalable quantum information processing, providing a robust foundation for developing sophisticated quantum algorithms and error correction technology necessary for practical, large-scale quantum systems.

Note added—We note other works on realizing remote two-qubit gates across superconducting quantum processors, such as the SWAP gate experimental implementation [43], a high-fidelity CNOT gate [44], and another theoretical protocol based on long-range ZZ interaction [45].

Acknowledgments—We thank Dr. He Wang, Dr. Kehuan Linghu, and Professor Shiping Zhao for their helpful discussions. We acknowledge the support from the National Natural Science Foundation of China (Grants No. 92365206, No. 12322413, No. 12404557, No. 12404560) and the Innovation Program for Quantum Science and Technology (No. 2021ZD0301802, No. 2023ZD0300200).

Data availability—The data that support the findings of this Letter are not publicly available upon publication because it is not technically feasible and/or the cost of preparing, depositing, and hosting the data would be prohibitive within the terms of this research project. The data are available from the authors upon reasonable request.

[1] F. Arute, K. Arya, R. Babbush, D. Bacon, J. C. Bardin, R. Barends, R. Biswas, S. Boixo, F. G. Brandao, D. A. Buell *et al.*, Quantum supremacy using a programmable superconducting processor, Nature (London) **574**, 505 (2019).

[2] Y. Wu, W.-S. Bao, S. Cao, F. Chen, M.-C. Chen, X. Chen, T.-H. Chung, H. Deng, Y. Du, D. Fan *et al.*, Strong quantum computational advantage using a superconducting quantum processor, Phys. Rev. Lett. **127**, 180501 (2021).

[3] G. Q. AI, Suppressing quantum errors by scaling a surface code logical qubit, Nature (London) **614**, 676 (2023).

[4] Y. Kim, A. Eddins, S. Anand, K. X. Wei, E. Van Den Berg, S. Rosenblatt, H. Nayfeh, Y. Wu, M. Zaletel, K. Temme *et al.*, Evidence for the utility of quantum computing before fault tolerance, Nature (London) **618**, 500 (2023).

[5] I. T. Rosen, S. Muschinske, C. N. Barrett, A. Chatterjee, M. Hays, M. DeMarco, A. Karamlou, D. Rower, R. Das, D. K. Kim, B. M. Niedzielski, M. Schuldt, K. Serniak, M. E. Schwartz, J. L. Yoder, J. A. Grover, and W. D. Oliver, A synthetic magnetic vector potential in a 2D superconducting qubit array, Nat. Phys. **20**, 1881 (2024).

[6] A. G. Fowler, M. Mariantoni, J. M. Martinis, and A. N. Cleland, Surface codes: Towards practical large-scale quantum computation, Phys. Rev. A **86**, 032324 (2012).

[7] M. Mohseni, A. Scherer, K. G. Johnson, O. Wertheim, M. Otten, N. A. Aadit *et al.*, How to build a quantum supercomputer: Scaling from hundreds to millions of qubits, arXiv:2411.10406.

[8] S. Bravyi, A. W. Cross, J. M. Gambetta, D. Maslov, P. Rall, and T. J. Yoder, High-threshold and low-overhead fault-tolerant quantum memory, Nature (London) **627**, 778 (2024).

[9] L. Jiang, J. M. Taylor, A. S. Sørensen, and M. D. Lukin, Distributed quantum computation based on small quantum registers, Phys. Rev. A **76**, 062323 (2007).

[10] C. Monroe, R. Raussendorf, A. Ruthven, K. R. Brown, P. Maunz, L.-M. Duan, and J. Kim, Large-scale modular quantum-computer architecture with atomic memory and photonic interconnects, Phys. Rev. A **89**, 022317 (2014).

[11] A. Gold, J. Paquette, A. Stockklauser, M. J. Reagor, M. S. Alam, A. Bestwick, N. Didier, A. Nersisyan, F. Oruc, A. Razavi *et al.*, Entanglement across separate silicon dies in a modular superconducting qubit device, npj Quantum Inf. **7**, 142 (2021).

[12] J. Ang *et al.*, Arquin: Architectures for multinode superconducting quantum computers, ACM Trans. Quantum Comput. **5**, 1 (2024).

[13] D. Main, P. Drmota, D. P. Nadlinger, E. M. Ainley, A. Agrawal, B. C. Nichol, R. Srinivas, G. Araneda, and D. M. Lucas, Distributed quantum computing across an optical network link, Nature (London) **638**, 383 (2025).

[14] A. Barenco, C. H. Bennett, R. Cleve, D. P. DiVincenzo, N. Margolus, P. Shor, T. Sleator, J. A. Smolin, and H. Weinfurter, Elementary gates for quantum computation, Phys. Rev. A **52**, 3457 (1995).

[15] N. Leung, Y. Lu, S. Chakram, R. K. Naik, N. Earnest, R. Ma, K. Jacobs, A. N. Cleland, and D. I. Schuster, Deterministic bidirectional communication and remote entanglement generation between superconducting qubits, npj Quantum Inf. **5**, 18 (2019).

[16] Y. P. Zhong, H. S. Chang, K. J. Satzinger, M. H. Chou, A. Bienfait, C. R. Conner, É. Dumur, J. Grebel, G. A. Peairs, R. G. Povey, D. I. Schuster, and A. N. Cleland, Violating Bell's inequality with remotely connected superconducting qubits, Nat. Phys. **15**, 741 (2019).

[17] P. Magnard, S. Storz, P. Kurpiers, J. Schär, F. Marxer, J. Lütolf, T. Walter, J.-C. Besse, M. Gabureac, K. Reuer *et al.*, Microwave quantum link between superconducting circuits housed in spatially separated cryogenic systems, Phys. Rev. Lett. **125**, 260502 (2020).

[18] P. Campagne-Ibarcq, E. Zalys-Geller, A. Narla, S. Shankar, P. Reinhold, L. Burkhart, C. Axline, W. Pfaff, L. Frunzio, R. J. Schoelkopf, and M. H. Devoret, Deterministic remote entanglement of superconducting circuits through microwave two-photon transitions, Phys. Rev. Lett. **120**, 200501 (2018).

[19] Y. Zhong, H.-S. Chang, A. Bienfait, É. Dumur, M.-H. Chou, C. R. Conner, J. Grebel, R. G. Povey, H. Yan, D. I. Schuster *et al.*, Deterministic multi-qubit entanglement in a quantum network, Nature (London) **590**, 571 (2021).

[20] H. Yan, Y. Zhong, H.-S. Chang, A. Bienfait, M.-H. Chou, C. R. Conner, É. Dumur, J. Grebel, R. G. Povey, and A. N. Cleland, Entanglement purification and protection in a superconducting quantum network, Phys. Rev. Lett. **128**, 080504 (2022).

[21] S. Storz, J. Schär, A. Kulikov, P. Magnard, P. Kurpiers, J. Lütolf, T. Walter, A. Copetudo, K. Reuer, A. Akin *et al.*, Loophole-free Bell inequality violation with superconducting circuits, Nature (London) **617**, 265 (2023).

[22] H.-S. Chang, Y. P. Zhong, A. Bienfait, M.-H. Chou, C. R. Conner, E. Dumur, J. Grebel, G. A. Peairs, R. G. Povey, K. J. Satzinger, and A. N. Cleland, Remote entanglement via adiabatic passage using a tunably dissipative quantum communication system, Phys. Rev. Lett. **124**, 240502 (2020).

[23] J. Niu, L. Zhang, Y. Liu, J. Qiu, W. Huang, J. Huang, H. Jia, J. Liu, Z. Tao, W. Wei *et al.*, Low-loss interconnects for modular superconducting quantum processors, National electronics review **6**, 235 (2023).
[24] Y. Makhlin, Nonlocal properties of two-qubit gates and mixed states, and the optimization of quantum computations, Quantum Inf. Process. **1**, 243 (2002).
[25] J. Zhang, J. Vala, S. Sastry, and K. B. Whaley, Geometric theory of nonlocal two-qubit operations, Phys. Rev. A **67**, 042313 (2003).
[26] P. Zanardi, C. Zalka, and L. Faoro, Entangling power of quantum evolutions, Phys. Rev. A **62**, 030301(R) (2000).
[27] J. Qiu, Y. Liu, L. Hu, Y. Wu, J. Niu, L. Zhang, W. Huang, Y. Chen, J. Li, S. Liu, Y. Zhong, L. Duan, and D. Yu, Deterministic quantum state and gate teleportation between distant superconducting chips, Sci. Bull. **70**, 351 (2025).
[28] M. Ohfuchi and S. Sato, Remote cross-resonance gate between superconducting fixed-frequency qubits, Quantum Sci. Technol. **9**, 035014 (2024).
[29] J. M. Chow, A. D. Córcoles, J. M. Gambetta, C. Rigetti, B. R. Johnson, J. A. Smolin, J. R. Rozen, G. A. Keefe, M. B. Rothwell, M. B. Ketchen, and M. Steffen, Simple all-microwave entangling gate for fixed-frequency superconducting qubits, Phys. Rev. Lett. **107**, 080502 (2011).
[30] A. D. Córcoles, J. M. Gambetta, J. M. Chow, J. A. Smolin, M. Ware, J. Strand, B. L. Plourde, and M. Steffen, Process verification of two-qubit quantum gates by randomized benchmarking, Phys. Rev. A **87**, 030301(R) (2013).
[31] S. Sheldon, E. Magesan, J. M. Chow, and J. M. Gambetta, Procedure for systematically tuning up cross-talk in the cross-resonance gate, Phys. Rev. A **93**, 060302(R) (2016).
[32] A. Kandala, K. X. Wei, S. Srinivasan, E. Magesan, S. Carnevale, G. A. Keefe, D. Klaus, O. Dial, and D. C. McKay, Demonstration of a high-fidelity cnot gate for fixed-frequency transmons with engineered *zz* suppression, Phys. Rev. Lett. **127**, 130501 (2021).
[33] K. X. Wei, E. Magesan, I. Lauer, S. Srinivasan, D. F. Bogorin, S. Carnevale, G. A. Keefe, Y. Kim, D. Klaus, W. Landers, N. Sundaresan, C. Wang, E. J. Zhang, M. Steffen, O. E. Dial, D. C. McKay, and A. Kandala, Hamiltonian engineering with multicolor drives for fast entangling gates and quantum crosstalk cancellation, Phys. Rev. Lett. **129**, 060501 (2022).
[34] B. K. Mitchell, R. K. Naik, A. Morvan, A. Hashim, J. M. Kreikebaum, B. Marinelli, W. Lavrijsen, K. Nowrouzi, D. I. Santiago, and I. Siddiqi, Hardware-efficient microwave-activated tunable coupling between superconducting qubits, Phys. Rev. Lett. **127**, 200502 (2021).
[35] See Supplemental Material, which includes Refs. [31,36–41], at http://link.aps.org/supplemental/10.1103/npr7-b7kq for additional information about experimental setups, numerical simulations and data analysis.
[36] C. Neill *et al.*, A blueprint for demonstrating quantum supremacy with superconducting qubits, Science **360**, 195 (2018),.
[37] G. J. Dolan, Offset masks for lift-off photoprocessing, Appl. Phys. Lett. **31**, 337 (1977).
[38] Z. Chen *et al.*, Measuring and suppressing quantum state leakage in a superconducting qubit, Phys. Rev. Lett. **116**, 020501 (2016).
[39] J. M. Gambetta, F. Motzoi, S. T. Merkel, and F. K. Wilhelm, Analytic control methods for high-fidelity unitary operations in a weakly nonlinear oscillator, Phys. Rev. A **83**, 012308 (2011).
[40] C. Shen and L.-M. Duan, Correcting detection errors in quantum state engineering through data processing, New J. Phys. **14**, 053053 (2012).
[41] P. D. Nation, H. Kang, N. Sundaresan, and J. M. Gambetta, Scalable mitigation of measurement errors on quantum computers, PRX Quantum **2**, 040326 (2021).
[42] J. F. Clauser, M. A. Horne, A. Shimony, and R. A. Holt, Proposed experiment to test local hidden-variable theories, Phys. Rev. Lett. **23**, 880 (1969).
[43] M. Mollenhauer, A. Irfan, X. Cao, S. Mandal, and W. Pfaff, A high-efficiency elementary network of interchangeable superconducting qubit devices, Natl. Electron. Rev. (2025). 10.1038/s41928-025-01404-3.
[44] K. Heya, T. Phung, M. Malekakhlagh, R. Steiner, M. Turchetti, W. Shanks, J. Mamin, W.-S. Lu, Y. P. Kandel, N. Sundaresan, and J. Orcutt, Randomized benchmarking of a high-fidelity remote cnot gate over a meter-scale microwave interconnect, arXiv:2502.15034.
[45] X. Deng, W. Zheng, X. Liao, H. Zhou, Y. Ge, J. Zhao, D. Lan, X. Tan, Y. Zhang, S. Li, and Y. Yu, Long-range *zz* interaction via resonator-induced phase in superconducting qubits, Phys. Rev. Lett. **134**, 020801 (2025).